The Astrophysical Journal, 976:177 (12pp), 2024 December 1 https://doi.org/10.3847/1538-4357/ad84f3

Tip of the Red Giant Branch Distances with JWST. II. *I*-band Measurements in a Sample of Hosts of 10 Type Ia Supernova Match HST Cepheids

Siyang Li[1], Gagandeep S. Anand[2], Adam G. Riess[1,2], Stefano Casertano[2], Wenlong Yuan[1], Louise Breuval[1], Lucas M. Macri[3], Daniel Scolnic[4], Rachael Beaton[1,2], and Richard I. Anderson[5]
[1] Department of Physics and Astronomy, Johns Hopkins University, Baltimore, MD 21218, USA; sli185@jh.edu
[2] Space Telescope Science Institute, 3700 San Martin Drive, Baltimore, MD 21218, USA
[3] NSF's NOIRLab, 950 N Cherry Avenue, Tucson, AZ 85719, USA
[4] Department of Physics, Duke University, Durham, NC 27708, USA
[5] Institute of Physics, École Polytechnique Fédérale de Lausanne (EPFL), Observatoire de Sauverny, 1290 Versoix, Switzerland
Received 2024 July 31; revised 2024 September 16; accepted 2024 September 19; published 2024 November 21

Abstract

The Hubble Tension, a $>5\sigma$ discrepancy between direct and indirect measurements of the Hubble constant (H_0), has persisted for a decade and motivated intense scrutiny of the paths used to infer H_0. Comparing independently derived distances for a set of galaxies with different standard candles, such as the tip of the red giant branch (TRGB) and Cepheid variables, can test for systematics in the middle rung of the distance ladder. The *I* band is the preferred filter for measuring the TRGB due to constancy with color, a result of low sensitivity to population differences in age and metallicity supported by stellar models. We use James Webb Space Telescope (JWST) observations with the maser host NGC 4258 as our geometric anchor to measure *I*-band (F090W versus F090W − F150W) TRGB distances to eight hosts of 10 Type Ia supernovae (SNe Ia) within 28 Mpc: NGC 1448, NGC 1559, NGC 2525, NGC 3370, NGC 3447, NGC 5584, NGC 5643, and NGC 5861. We compare these with Hubble Space Telescope (HST) Cepheid-based relative distance moduli for the same galaxies and anchor. We find no evidence of a difference between their weighted means, 0.01 ± 0.04 (stat) ± 0.04 (sys) mag. We produce 14 variants of the TRGB analysis, altering the smoothing level and color range used to measure the tips to explore their impact. For some hosts, this changes the identification of the strongest peak, but this causes little change to the sample mean difference, producing a full range of 0.00–0.02 mag, all consistent at 1σ with no difference. The result matches past comparisons of *I*-band TRGB and Cepheids when both use HST. SNe and anchor samples observed with JWST are too small to yield a measure of H_0 that is competitive with the HST sample of 42 SNe Ia and 4 anchors; however, they already provide a vital systematic cross-check to HST measurements of the distance ladder.

Unified Astronomy Thesaurus concepts: Distance indicators (394); Galaxy distances (590); Hubble constant (758); Red giant tip (1371); James Webb Space Telescope (2291); Cepheid variable stars (218); Standard candles (1563); Observational cosmology (1146); Luminosity function (942); Red giant stars (1372)

1. Introduction

The "Hubble Tension" refers to a 5σ–6σ discrepancy between direct measurements and cosmological inference of the present expansion rate of the Universe, parameterized as the Hubble constant (H_0). Currently, the "gold standard" method to directly measure H_0 utilizes a three-rung ladder to obtain distances to galaxies in the Hubble flow. This method uses geometric distances derived from parallaxes (such as those from Gaia Collaboration et al. 2021), water masers (M. J. Reid et al. 2019), and detached eclipsing binaries (G. Pietrzyński et al. 2019; D. Graczyk et al. 2020) to calibrate the luminosities of primary distance indicators such as Cepheid variables (first rung). This calibration is in turn used to measure distances to galaxies that host both Cepheids and Type Ia supernovae (SNe Ia) to calibrate the luminosities of the latter (second rung), which are then finally used to measure distances to galaxies in the Hubble flow to measure H_0 (third rung). The Supernovae, H_0, for the Equation of State team, for instance, has used this method to measure $H_0 = 73.17 \pm 0.86\,\mathrm{km\,s^{-1}\,Mpc^{-1}}$ (A. G. Riess et al. 2022; L. Breuval et al. 2024). The cosmological inference uses the cosmic microwave background together with a cosmological model such as ΛCDM to infer the present expansion rate. Planck Collaboration et al. (2020) used this approach to derive $H_0 = 67.36 \pm 0.54\,\mathrm{km\,s^{-1}\,Mpc^{-1}}$, a $>5\sigma$ difference from the value obtained by L. Breuval et al. (2024). Several independent teams and measurements using a wide range of distance indicators have also yielded measurements in tension with those from Planck. No precise direct measurement of H_0 has yielded a value that is lower than that from Planck (see compilations in E. Di Valentino et al. 2021; L. Verde et al. 2024). This tension suggests a possible need to revise the standard ΛCDM model, though efforts continue to search for unidentified systematics in the measurements at any level.[6]

Independent distance measurements to the same galaxies using multiple standard candles offers one of the best ways to ensure systematics are well accounted for and understood. The

[6] For an extensive list of studies that have studied systematics related to the tension, we refer the reader to https://djbrout.github.io/SH0ESrefs.html.

tip of the red giant branch (TRGB) refers to the maximum luminosity reached by first-ascent red giant stars before transitioning onto the horizontal branch and has been used as a standard candle to measure distances (e.g., G. S. Anand et al. 2019a, 2019b, 2021a, 2021b, 2024a, 2024b; R. L. Beaton et al. 2019; T. J. Hoyt et al. 2021; A. J. Lee et al. 2021b, 2022; E. K. Oakes et al. 2022; Q. H. Tran et al. 2022; B. F. Madore & W. L. Freedman 2024) and the Hubble constant (e.g., W. L. Freedman et al. 2019; Y. J. Kim et al. 2020; W. L. Freedman 2021; J. P. Blakeslee et al. 2021; G. S. Anand et al. 2022; S. Dhawan et al. 2022, 2023; D. Scolnic et al. 2023, see also the review in E. Di Valentino & D. Brout 2024). The TRGB can thus be used as a means to cross-check systematics of other standard candles, such as Cepheid variables.

The TRGB is commonly measured in the I band, or the Hubble Space Telescope (HST) F814W and James Webb Space Telescope (JWST) F090W equivalents, where the magnitude of the TRGB exhibits the smallest metallicity (and hence color) dependence (L. Rizzi et al. 2007; I. S. Jang & M. G. Lee 2017a). While it is possible to measure the TRGB in the near-infrared (NIR) to take advantage of brighter magnitudes, doing so requires careful calibration of the TRGB's color dependence (M. Bellazzini et al. 2004; J. J. Dalcanton et al. 2012; P.-F. Wu et al. 2014; T. J. Hoyt et al. 2018; B. F. Madore et al. 2018; K. B. W. McQuinn et al. 2019; T. J. Hoyt et al. 2024; M. J. B. Newman et al. 2024a, 2024b), where it rises to $\sim$1 magnitude per magnitude of measured color, introducing additional systematics. In this study, we focus on measuring the TRGB in the JWST F090W filter, which is most similar to I and F814W used with HST.

The launch of JWST has opened up the possibility of performing extensive cross-checks of Cepheids, TRGB, and other standard candles in unprecedented resolution. In particular, the dual-module configuration of the JWST NIRCam instrument allows for at least three standard candles (Cepheids, TRGB, and carbon stars) to be simultaneously observed with one set of observations—see, for instance, JWST programs GO-1685 (A. Riess et al. 2021), GO-1995 (W. L. Freedman et al. 2021), and GO-2875 (A. Riess et al. 2023), among others. In a previous study (G. S. Anand et al. 2024a; hereafter Paper I), we measured the TRGB with JWST in the maser host NGC 4258, which serves as one of four geometric calibrators of the distance ladder, and presented measurements two 2 SN Ia hosts (NGC 1559 and NGC 5584). The derived luminosity of the TRGB in JWST F090W in Paper I matched that independently determined by M. J. B. Newman et al. (2024a), also in F090W, to $\pm$0.01 mag, indicating a reliable foundation for distance measurements with JWST in SN Ia hosts. Here we study an expanded sample using JWST observations of eight hosts of 10 SNe Ia from Cycle 1 program GO-1685 (A. Riess et al. 2021) and Cycle 2 GO-2785 (A. Riess et al. 2023) to measure TRGB-based distances to these galaxies and test their consistency with HST Cepheid-based distances to those same galaxies.

2. Data

We retrieve JWST F090W and F150W observations of NGC 1448, NGC 1559, NGC 5584, and NGC 5643 from GO-1685 (A. Riess et al. 2021) and NGC 2525, NGC 3370, NGC 3447, and NGC 5861 from GO-2875 (A. Riess et al. 2023) using the Barbara A. Mikulski Archive for Space Telescopes.[7] We list observation details in Table 1 and show galaxy footprints in Figure 1. For NGC 2525, we found that the images corresponding to the fourth (and final) dither for each filter were noticeably blurred. Upon further investigation, we found that the guide star had wandered onto some bad pixels in the Fine Guidance Sensor. We thus excluded these dithers from our analysis and generated our own stage 3 image from only the first three dithers for use of mutual image alignment of the underlying stage 2 images with DOLPHOT.

3. Photometry

We follow the general procedures outlined by previous works from our team for photometric reductions (Paper I; A. G. Riess et al. 2024a). In detail, we perform point-spread function (PSF) photometry[8] using the DOLPHOT[9] software package (A. E. Dolphin 2000; A. Dolphin 2016), together with the latest (2024 February) version of the JWST/NIRCam module (D. R. Weisz et al. 2024). We use the stage 3 F150W `i2d` files as reference frames and perform photometry directly on the stage 2 `cal` images. We use the Vega–Vega system to remain consistent with earlier versions of DOLPHOT's JWST module, which gives a $\sim$0.04 mag offset (in F090W) from the Vega–Sirius system that is currently default in DOLPHOT NIRCam module. We use the "-etctime" option, which allows the package to use (`TMEASURE`) for signal-to-noise ratio (S/N) calculations. We apply the following DOLPHOT quality cuts, similar to those from D. R. Weisz et al. (2024): `crowd` < 0.5 (in both bands), `sharp`$^2 < 0.01$ (in both bands), and `type` $\leqslant$2. In addition to these quality cuts, we also apply S/N cuts in both bands for each target. For NGC 1448, NGC 1559, NGC 3447, NGC 5584, and NGC 5643, we adopt a minimum threshold of `S/N` $= 5$, whereas we choose a value of `S/N` $= 3$ for NGC 2525, NGC 3370, and NGC 5861 (due to the decreased relative depth of their photometry).

We also correct for foreground extinction using $E(B-V)$ from E. F. Schlafly & D. P. Finkbeiner (2011) and galaxy coordinates, both retrieved using the the NASA/IPAC Extragalactic Distance Database (NED)[10] and listed in Table 2, and the TRGB color selection has been adjusted to account for the reddening correction. We use the E. L. Fitzpatrick (1999) reddening law with $R_v = 3.1$ and $A_\lambda/E(B-V) = 1.4156$ and 0.6021 for F090W and F150W, respectively (Paper I). We adopt the extinction used in G. S. Anand et al. (2022) of $E(B-V) = 0.161$ mag for NGC 5643, which is located at a low galactic latitude (where the dust maps are less certain) and where the adopted value was reestimated using the displacement of the zero-age main sequence following L. Rizzi et al. (2017).

4. Measurement

Measuring the TRGB magnitude involves locating the discontinuity or inflection point of the luminosity function consisting of red giant and asymptotic giant branch stars. This can be done in many ways; for instance, using a Sobel filter (M. G. Lee et al. 1993; D. Hatt et al. 2017) or model-based

[7] https://mast.stsci.edu/portal/Mashup/Clients/Mast/Portal.html

[8] The photometry for this study is available publicly in a Zenodo repository, doi:10.5281/zenodo.13131990.

[9] http://americano.dolphinsim.com/dolphot/

[10] https://ned.ipac.caltech.edu/

Table 1
Summary Table for the JWST NIRCam Observations of NGC 1448, NGC 1559, NGC 2525, NGC 3370, NGC 3447, NGC 5584, NGC 5643, and NGC 5861 Used in This Study

Galaxy	Program	Observation Number	Observation Date	Filters	Exposure Time (s)	pmap Version
NGC 1448	GO-1685	13	2023-08-02	F090W/F277W	418.7 × 4	1215
NGC 1448	GO-1685	13	2023-08-02	F150W/F277W	526.1 × 4	...
NGC 1448	GO-1685	14	2023-18-02	F090W/F277W	418.7 × 4	...
NGC 1448	GO-1685	14	2023-18-02	F150W/F277W	526.1 × 4	...
NGC 1559	GO-1685	1	2023-06-30	F090W/F277W	418.7 × 4	...
NGC 1559	GO-1685	1	2023-06-30	F150W/F277W	526.1 × 4	...
NGC 1559	GO-1685	2	2023-07-15	F090W/F277W	418.7 × 4	...
NGC 1559	GO-1685	2	2023-07-15	F150W/F277W	526.1 × 4	...
NGC 5584	GO-1685	9	2023-01-30	F090W/F277W	418.7 × 4	...
NGC 5584	GO-1685	9	2023-01-30	F150W/F277W	526.1 × 4	...
NGC 5584	GO-1685	10	2023-02-21	F090W/F277W	418.7 × 4	...
NGC 5584	GO-1685	10	2023-02-21	F150W/F277W	526.1 × 4	...
NGC 5643	GO-1685	11	2023-07-07	F090W/F277W	311.4 × 4	...
NGC 5643	GO-1685	11	2023-07-07	F150W/F277W	418.7 × 4	...
NGC 5643	GO-1685	12	2023-07-22	F090W/F277W	311.4 × 4	...
NGC 5643	GO-1685	12	2023-07-22	F150W/F277W	418.7 × 4	...
NGC 2525	GO-2875	1	2023-04-23	F090W/F277W	472.4 × 3	1225
NGC 2525	GO-2875	1	2023-04-23	F150W/F277W	526.1 × 3	...
NGC 3370	GO-2875	2	2023-06-28	F090W/F277W	472.4 × 4	1234
NGC 3370	GO-2875	2	2023-06-28	F150W/F277W	526.1 × 4	...
NGC 3447	GO-2875	12	2023-05-24	F090W/F277W	472.4 × 4	...
NGC 3447	GO-2875	12	2023-05-24	F150W/F277W	622.7 × 4	...
NGC 5861	GO-2875	14	2024-07-30	F090W/F277W	472.4 × 4	...
NGC 5861	GO-2875	14	2024-07-30	F150W/F277W	622.7 × 4	...

Note. Columns from left to right: galaxy name, program number, observation number, observation date, filters, exposure time per dither, and context (pmap) file version.

methods, with either least-squares fitters (P.-F. Wu et al. 2014; D. Crnojević et al. 2019) or maximum-likelihood estimation (D. Makarov et al. 2006; S. Li et al. 2022, 2023a). In this study, we measure the TRGB using a Sobel filter using the measurement routine without spatial clipping (which we instead perform using elliptical annuli) from the Comparative Analysis of TRGBs (CATs) team (S. Li et al. 2023b; D. Scolnic et al. 2023; J. Wu et al. 2023), which is publicly available on GitHub.[11] The CATs team had optimized their measurement parameters (such as smoothing value, color cuts, etc.) by minimizing field-to-field dispersion in the TRGB measurement across multiple fields. At the moment, there are a limited number of JWST fields in each host galaxy, which prevents us from performing a similar optimization. For this study, we adopt a smoothing value of 0.05 mag and unweighted or "simple" weighting, as named in the CATs algorithm (i.e., no further weighting of the output of the edge-detection measurement). We note that without the CATs optimizations in place, this methodology is equivalent to the TRGB measurements adopted by the Carnegie-Chicago Hubble Program (CCHP; R. L. Beaton et al. 2016; W. L. Freedman et al. 2019), but without the additional weighting of the Sobel filter output (which has been shown to cause biases in the outputs; Paper I; R. I. Anderson et al. 2024). We explore the effects of varying the level of smoothing of the luminosity function and the color range used to measure the luminosity function, 14 combinations in all, in the next section. TRGB uncertainties are estimated using bootstrap resampling of the luminosity function with 5000 samples and the standard deviation of the bootstrap distribution. These distributions all follow Gaussianity with means that lie within 1σ from the measured TRGB. For NGC 5584, using the smaller smoothing value of $s = 0.05$ mag produces a Sobel response that shows two peaks of nearly the same height. Following G. S. Anand et al. (2024a), if there are two Sobel peaks that are of equivalent height ($\leqslant 3\%$), we select the brighter peak. The bootstrap distribution for NGC 5584 exhibits two Gaussians corresponding to the two Sobel peaks in the baseline result. We incorporate this spread to account for uncertainty in peak selection for NGC 5584.

Before measuring the TRGB, we perform spatial selections to limit contamination from younger stellar populations in these star-forming galaxies. The NIRCam regions used to measure

[11] https://github.com/JiaxiWu1018/Unsupervised-TRGB

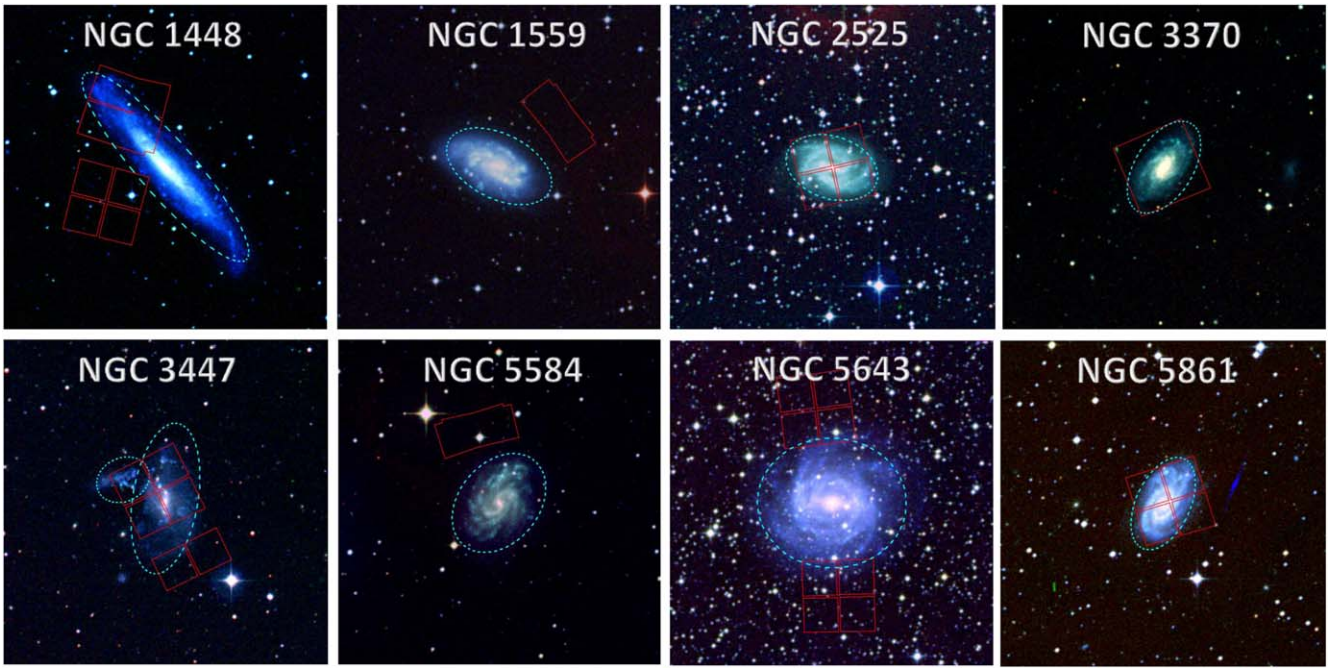

Figure 1. Footprints of the portions of the JWST/NIRCam visits used for our analysis (see the main text for details of our spatial selections) overlaid on $10' \times 10'$ images from the Digitized Sky Survey. The cyan dashed lines show D_{25} (except for NGC 3447, which is an interacting system), and we remove any stars within this region from our catalogs prior to our measurements.

the TRGB are highlighted in Figure 1—in all cases (except NGC 3447, described below), only regions exterior to the $B = 25$ mag arcsec^{-2} isophote (D_{25}; G. de Vaucouleurs et al. 1991) are selected (G. S. Anand et al. 2022, 2024a; T. J. Hoyt et al. 2024). For NGC 1559 and NGC 5584, the parallel NIRCam module contains a suitable sampling of stars, although only half of the parallel module is used (the far half of each contains too few stars to perform precise empirical PSF adjustments and aperture corrections). The same is nearly true for NGC 5643, though we remove a small portion of each parallel module that is interior to D_{25}. In NGC 1448, NGC 2525, NGC 3370, and NGC 5861, a sizeable portion of the main module is outside of D_{25}, which we include to increase the sampling of stars, and for NGC 2525, NGC 3370, and NGC 5861, the parallel modules contain too few stars to perform photometry on. Lastly, NGC 3447 is an actively interacting system, often described as two targets, N3447A and B. Here, we use two ellipses centered at R.A., decl. = (10:53:23.998, +16:46:26.78) and (10:53:29:3934, +16:47:02.294), major axes of 140″ and 50″, minor axes of 60″ and 40″, and position angles of 80° and 115°, respectively, following P. Mazzei et al. (2018).

A color image of NGC 3370 is shown in Figure 2, along with the same D_{25} selection region adopted for the spatial cuts. It can be seen that the outer regions of the image used for our analysis are of low stellar density, where stars are easily separated. While in some cases the TRGB is only ∼1 mag above the photometric completeness limit, we note that our spatial selection criteria as described above limit the effects of photometric bias, which would otherwise skew our edge-detection measurements in higher surface-brightness regions. Even for galaxies where the TRGB is located closest to the photometric limit, we do not measure any noticeable photometric bias in our selected halo regions—for example, the TRGB in NGC 3370 lies near a photometric completeness of ∼65%, but the measured photometric bias remains negligible (<0.01 mag).

The TRGB in F090W is expected to have minimal variation (<0.02 mag) with color over a range of $1.15 < \mathrm{F090W} - \mathrm{F150W} < 1.75$ mag (Paper I). Here, we adopt a color selection of $1.30 < \mathrm{F090W} - \mathrm{F150W} < 1.75$ mag for our baseline result (see Figure 2 in Paper I), where the tighter range aims to limit the effects of a limited amount of supergiants, which remain in our color–magnitude diagrams.

5. Distances

We use the TRGB measurements shown in Figure 3 to measure distances to the host galaxies. We adopt a TRGB zero point of $M_{\mathrm{TRGB}}^{\mathrm{F090W}} = -4.372 \pm 0.033$ (stat) $\pm$ 0.045 (sys) mag from G. S. Anand et al. (2024a)—based on $m_{\mathrm{TRGB}} =$ 25.045 mag, which is the mean of the two simple Sobel measurements using a $D > D_{25}$ and outer spatial selections (either being within $\pm$ 0.005 mag of this mean). This calibration uses the geometric maser distance to NGC 4258 (M. J. Reid et al. 2019) to calibrate the TRGB in the JWST F090W system and is stable for smoothing values $s = 0.04$ mag to $s = 0.12$ mag due to the absence of weighting (see Figure 6 in Paper I). This absolute calibration is also highly consistent with the independently derived zero point of $M_{\mathrm{TRGB}}^{\mathrm{F090W}} = -4.36 \pm 0.025$ (stat) $\pm$ 0.043 (sys) mag from M. J. B. Newman et al. (2024b), after adjusting their value from the Sirius–Vega system to the Vega–Vega zero-point system (M. Newman 2024, private communication). We list and plot the distances to the host galaxies, compared to Cepheid-based distances from A. G. Riess et al. (2022). We compare to fit variant 10 from A. G. Riess et al. (2022) for consistency in anchor selection; the distances produced by fit variant 10 are on average greater than those using all anchors (baseline) by ∼0.015 mag, consistent with their

Table 2
TRGB and Cepheid Distances to NGC 1448, NGC 1559, NGC 2525, NGC 3370, NGC 3447, NGC 5584, and NGC 5643

Galaxy	$E(B-V)$	R	NBT	TRGB $s=0.10$	σ $s=0.10$	TRGB $s=0.05$	σ $s=0.05$	ΔTRGB ($s=0.10-s=0.05$)	μ_0(TRGB) $s=0.10$	σ $s=0.10$	μ_0(TRGB) $s=0.05$	σ $s=0.05$	μ_0 Cepheid	σ Cepheid	σ (var)
NGC 1448	0.012	3.2	7392	26.97	0.02	27.02	0.05	−0.05	31.34	0.05	31.39	0.07	31.30	0.05	0.02
NGC 1559	0.026	3.8	1582	27.13	0.01	27.14	0.01	−0.01	31.50	0.05	31.51	0.05	31.50	0.07	0.01
NGC 2525	0.052	2.1	8225	27.50	0.03	27.44	0.07	0.06	31.87	0.06	31.81	0.09	32.06	0.11	0.04
NGC 3370	0.028	1.7	617	27.82	0.03	27.82	0.07	0	32.19	0.06	32.19	0.08	32.13	0.06	0.02
NGC 3447	0.026	1.9	678	27.56	0.04	27.55	0.08	0.01	31.93	0.06	31.92	0.09	31.95	0.05	0.01
NGC 5584	0.035	2.6	1582	27.58	0.06	27.43	0.10	0.15	31.95	0.08	31.8	0.11	31.77	0.06	0.07
NGC 5643	0.161	3.2	21032	26.20	0.01	26.21	0.01	−0.01	30.57	0.06	30.58	0.06	30.55	0.06	0.01
NGC 5861	0.095	1.5	6199	27.73	0.03	27.73	0.10	0	32.10	0.06	32.10	0.11	32.23	0.11	0.02

Note. Cepheid distances are from A. G. Riess et al. (2022), fit variant 10. Distance errors do not include an 0.032 mag uncertainty from the maser distance for either Cepheids or TRGB. TRGB distances include a (correlated across the host galaxies) measurement error for NGC 4258 of 0.045 mag from G. S. Anand et al. (2024a). We adopt 15% of the extinction value as a systematic uncertainty unless it is less than 0.01 mag, in which case we instead adopt a full $1/2$ of the extinction value as the uncertainty. We also add in quadrature a systematic uncertainty from measurement and peak choices with values and measurement variants listed in Tables 2 and 3, respectively. Columns from left to right: (1) galaxy name, (2) $E(B-V)$ from NED, (3) contrast ratio (R) defined from J. Wu et al. (2023), (4) number of stars 1 magnitude fainter than the measured TRGB (NBT) with smoothing $s=0.05$ mag, (5) TRGB measured here with a smoothing value of 0.10 mag, (6) error on that TRGB measurement, (7) TRGB measured here with a smoothing value of 0.05 mag, (8) error on that TRGB measurement, (9) difference between the TRGBs measured with $s=0.05$ and $s=0.10$ mag, (10) TRGB distance modulus measured here using a smoothing value of 0.10 mag, (11) error on that TRGB distance modulus, (12) TRGB distance modulus measured here using a smoothing value of 0.05 mag, (13) error on that TRGB distance modulus, (14) Cepheid distance (fit variant 10; A. G. Riess et al. 2022), (15) error on the Cepheid distance, (16) dispersion of variants (measurement choices), which may be considered as a systematic error on an individual distance measurement (Table 3).

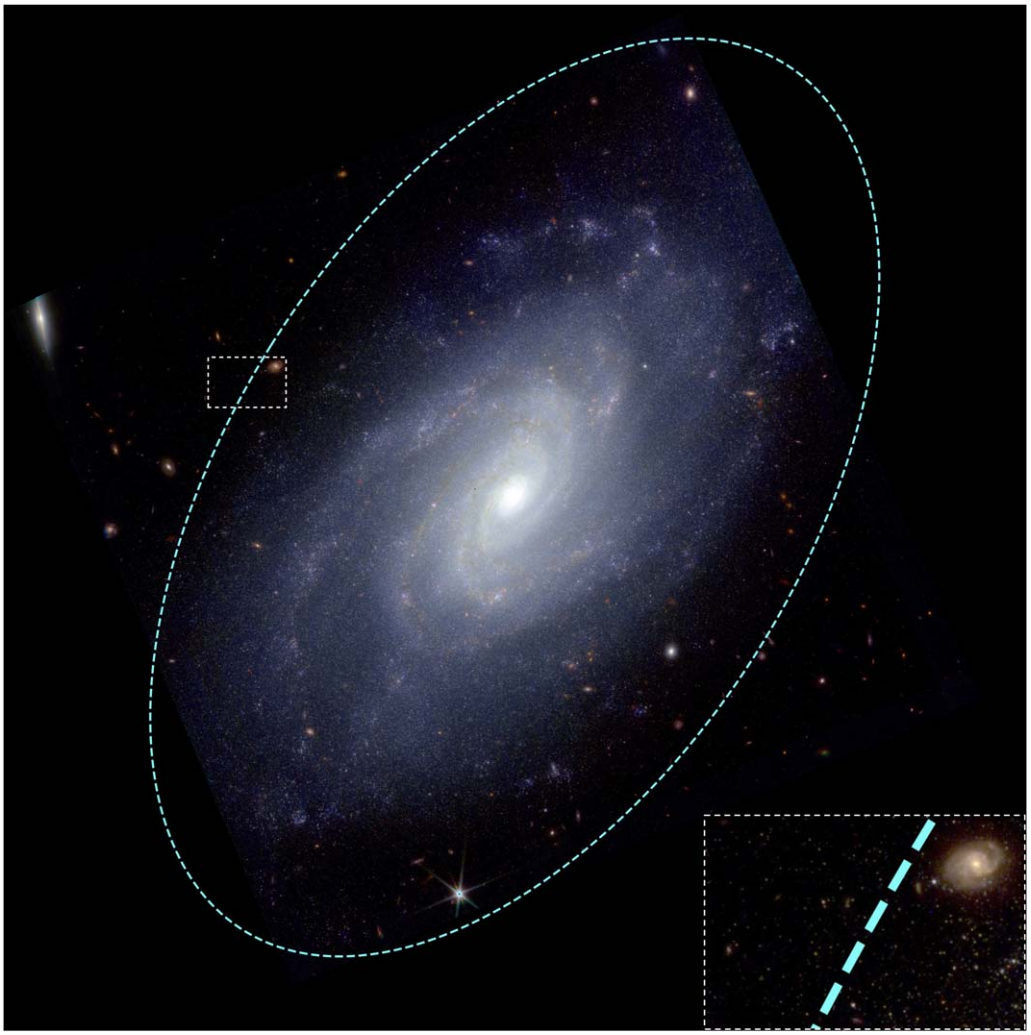

Figure 2. Color image of NGC 3370 generated from our F090W + F150W + F277W JWST/NIRCam imaging. D_{25} ($B = 25$ mag arcsec^{-2} isophote) is shown as the cyan dashed line—only stars outside of this region are included in our TRGB analysis. A dashed white inset shows a zoom-in on a region near the selected isophote (the color inset image is displayed with a tighter dynamic range to more clearly show stars in the halo).

differences in H_0 of 72.5 km s^{-1} Mpc^{-1} for NGC 4258 and 73.0 km s^{-1} Mpc^{-1} using all anchors.

We find a weighted mean difference between the TRGB (baseline results with $1.30 <$ F090W − F150W < 1.75 mag and smoothing of $s = 0.05$ mag) and HST Cepheid distances of 0.01 ± 0.04 (stat) ± 0.04 (sys) mag, which includes the systematic error due to measurement choice listed in Table 2, between the TRGB distance moduli measured here and Cepheid distance moduli from HST. We find no statistically significant difference between the two sets of distances measured between the same anchor and SN Ia hosts but with independent distance indicators. We have not attempted to account for any further population-based differences intrinsic to the TRGB between the field of NGC 4258 and the mean of the SN Ia hosts but believe these are limited due to the limited metallicity and age differences expected in F090W and our restricted color window (Paper I).

The choice of algorithm and selection parameters can impact final TRGB measurements. One compelling approach is to optimize the measurement parameters to minimize scatter in the field-to-field variations (see S. Li et al. 2023b; D. Scolnic et al. 2023; J. Wu et al. 2023); however, the limited number of JWST fields available to measure the TRGB within our host galaxies prevents us from performing such an optimization. To investigate the effects of how different parameter choices can impact our measurements, we explore 14 combinations of different luminosity function smoothing, color selection, and zero-point choice. We list the different measurement variants explored in this analysis, together with the weighted mean difference between the TRGB and HST Cepheid distances for each variant, in Table 3. We include a thirteenth variant using the zero-point from M. J. B. Newman et al. (2024b), adjusted for the Vega−Vega photometric system, which has differences of ∼0.04 mag in F090W and ∼0.02 mag in F150W. We also add a fourteenth variant where we use the median of all TRGB measurements (three smoothings, four color ranges) to compare with Cepheids. We add the standard deviation of the measured TRGBs across the smoothing and color range variants for each galaxy, excluding the variants using the zero point from M. J. B. Newman et al. (2024b) and median TRGB, as a systematic error to our measurements, listed in Table 2. We find that for all variants, the mean differences between the TRGB and Cepheid distances across all galaxies for a given variant are consistent with zero within their statistical uncertainties with a full range of 0.00–0.02 mag.

Table 3
Summary Table for the Weighted Mean Differences between the TRGB and Cepheid Distances (TRGB − Cepheid) to NGC 1448, NGC 1559, NGC 2525, NGC 3370, NGC 3447, NGC 5584, NGC 5643, and NGC 5861 across Various Measurement Variants

Smoothing (mag)	Color Cuts (mag)	$\tilde{\mu}_{\mathrm{TRGB-Cepheid}}$ (mag)	σ (mag)	Calibration	χ^2	Weighted Scatter (mag)
0.05	1.15, 1.65	0.022	0.034	G. S. Anand et al. (2024a)	1.103	0.10
0.05	1.15, 1.75	0.018	0.034	G. S. Anand et al. (2024a)	1.363	0.11
0.05	**1.30, 1.75**	**0.007**	**0.037**	G. S. Anand et al. (2024a)	**0.712**	**0.09**
0.07	1.15, 1.65	0.014	0.033	G. S. Anand et al. (2024a)	1.008	0.09
0.07	1.15, 1.75	0.014	0.033	G. S. Anand et al. (2024a)	1.317	0.11
0.07	1.30, 1.75	0.013	0.034	G. S. Anand et al. (2024a)	1.083	0.10
0.10	1.15, 1.65	0.011	0.031	G. S. Anand et al. (2024a)	1.057	0.09
0.10	1.15, 1.75	0.015	0.031	G. S. Anand et al. (2024a)	1.121	0.09
0.10	1.30, 1.75	0.014	0.032	G. S. Anand et al. (2024a)	0.961	0.09
0.10	1.30, 1.75	0.005	0.032	M. J. B. Newman et al. (2024b)	0.882	0.08
0.15	1.15, 1.65	0.007	0.031	G. S. Anand et al. (2024a)	1.139	0.09
0.15	1.15, 1.75	0.014	0.030	G. S. Anand et al. (2024a)	1.138	0.09
0.15	1.30, 1.75	0.012	0.031	G. S. Anand et al. (2024a)	1.015	0.09
All Smoothings	All Color Ranges	0.008	0.031	G. S. Anand et al. (2024a)	0.996	0.09

Note. Cepheid distances are from A. G. Riess et al. (2022), fit variant 10. The error in the mean difference, TRGB − Cepheid, does not include a systematic uncertainty of 0.03 mag for the TRGB measurement error in NGC 4258 from G. S. Anand et al. (2024a). Measurements use "simple" smoothing (i.e., no weighting; see J. Wu et al. 2023) and do not include the measurement choice error listed in Table 2, except for the last variant that uses the median TRGB across all smoothing and color range variants. Bold values correspond to the baseline variant that uses $s = 0.05$ mag smoothing with a color range of $1.3 < \mathrm{F090W} - \mathrm{F150W} < 1.75$ mag. For the variant that uses the M. J. B. Newman et al. (2024b), we use the errors listed in their Tables 4 and 6 added in quadrature with the TRGB measurement and foreground extinction errors. Columns from left to right: smoothing value, color cuts, mean difference between TRGB and Cepheid distances, error on the mean difference, calibration, χ^2, and weighted scatter.

In Figure 4, the error in the mean μ_{TRGB}–μ_{Cepheid} of 0.03–0.04 mag is a statistical uncertainty. There is also a systematic uncertainty in the mean TRGB and Cepheid comparison from the measurement uncertainty of the TRGB in NGC 4258 of ±0.04 mag (Paper I), which pertains to all calibrated TRGB distances and likewise for Cepheids in NGC 4258 of ±0.02 mag or ±0.045 mag when they are combined. This systematic term due to the measurement of NGC 4258 for both methods is the dominant term in the comparison and may only be reduced in the future with the use of additional observations of NGC 4258. The maser distance uncertainty of ±0.032 mag should not be considered in this distance comparison as it is common to both the Cepheid and TRGB distances.

We can also compare the distances to NGC 1559 and NGC 5584 from G. S. Anand et al. (2024a), who used the same data set as here. G. S. Anand et al. (2024a) found distances of $\mu_0 = 31.49 \pm 0.07$ mag ($\Delta = 0.02$ mag) and 31.80 ± 0.08 mag ($\Delta = 0.00$ mag) to NGC 1559 and NGC 5584, respectively, when comparing their results to ours from the same smoothing scale (for NGC 1559, we now have combined both visits to obtain higher S/N photometry). The TRGB distance for NGC 1559 is also in agreement with that measured with Miras in C. D. Huang et al. (2020) of $\mu_0 = 31.41 \pm 0.050 \pm 0.060$ mag.

An unavoidable feature of the TRGB method of edge detection is a potential ambiguity when multiple Sobel peaks of similar height are present. For NGC 5584 there are two Sobel peaks separated by 0.2–0.3 mag. Because the peaks are similar in height, different measurement choices may cause changes in which peak is higher. To account for this possibility, we provide an additional individual distance uncertainty listed in Table 2 estimated from the variation of individual results of variants in Table 3. This uncertainty should be added for citing a single distance estimate for each host. A similar situation involving two peaks at similar heights but at a smaller level, 0.05 mag, is seen for NGC 1448 and in the reverse direction for NGC 2525.

Table 4
Summary Table for Distances to NGC 1448 and NGC 5643 from EDD (G. S. Anand et al. 2021b), CCHP (W. L. Freedman 2021), and Here

Galaxy	References	μ_0(TRGB)
NGC 1448	G. S. Anand et al. (2021b)	31.38
NGC 1448	W. L. Freedman (2021)	31.32
NGC 1448	Here	31.39 ($s = 0.05$), 31.34 ($s = 0.10$)
NGC 5643	G. S. Anand et al. (2021b)	30.47
NGC 5643	W. L. Freedman (2021)	30.48
NGC 5643	Here	30.58 ($s = 0.05$), 30.57 ($s = 0.10$)

The Extragalactic Distance Database (EDD; G. S. Anand et al. 2021b) and CCHP (W. L. Freedman 2021) teams have measured HST TRGB distances to NGC 1448 and NGC 5643, which can provide an interesting comparison with the JWST distances found here. These distances also reflect differences in the TRGB measurement methodology; the EDD team uses a model-based approach (D. Makarov et al. 2006; P.-F. Wu et al. 2014), while the CCHP team uses a Sobel filter applied on a Gaussian-windowed, locally weighted scatterplot smoothing-smoothed luminosity function (D. Hatt et al. 2017). We list this comparison in Table 4. For NGC 1448, these teams independently found distance moduli of 31.38 (EDD) and 31.32 mag (CCHP), compared to 31.34 and 31.39 mag (different levels of smoothing) found here, resulting in a standard deviation of 0.03 mag. For NGC 5643, these team found 30.47 (EDD) and 30.48 mag (CCHP), compared to 30.57 and 30.58 mag (which agrees well with Cepheids) found here, resulting in a standard deviation of 0.05 mag.

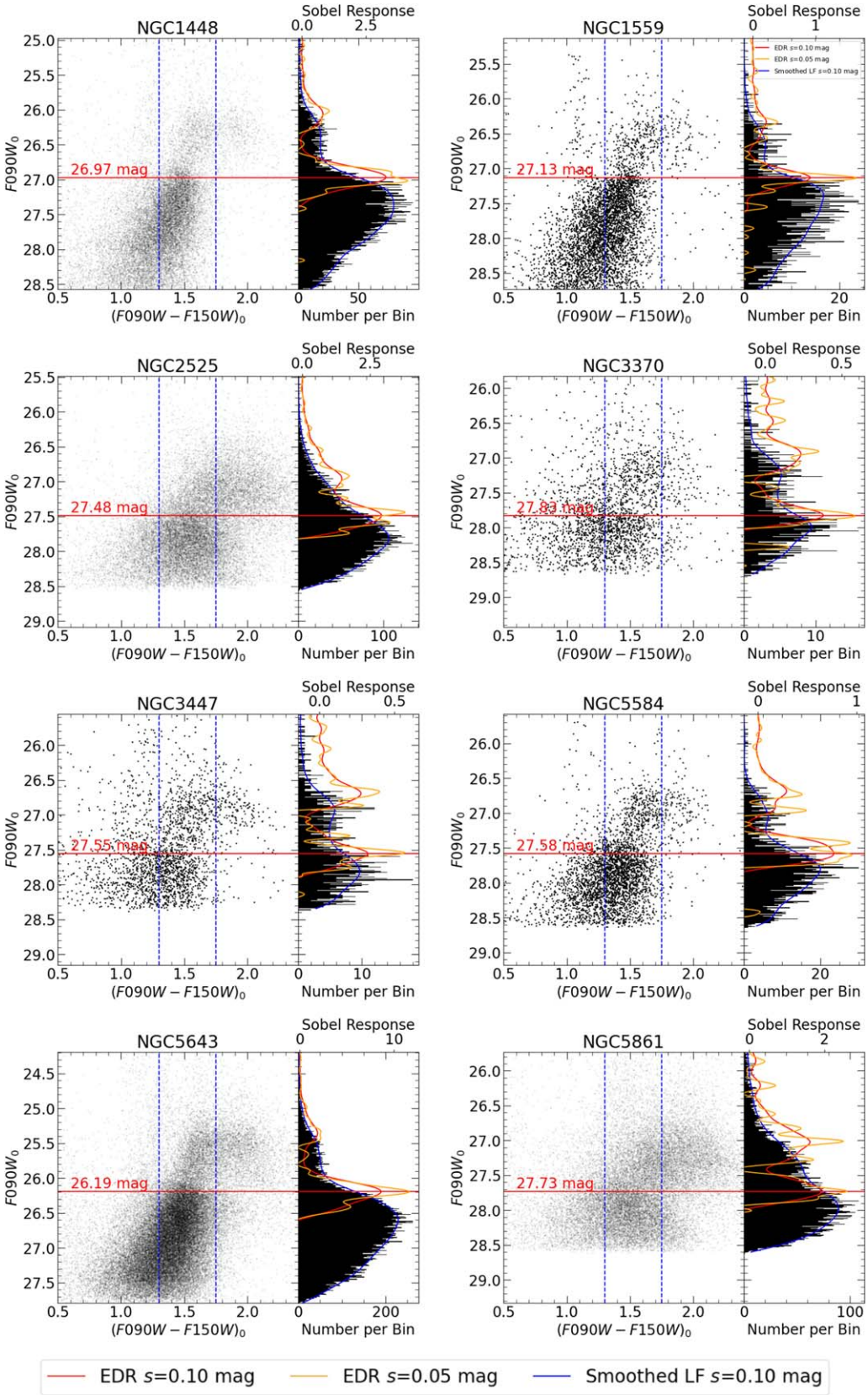

Figure 3. Color–magnitude diagrams and luminosity functions used for the TRGB measurements in this study. The vertical blue dashed lines show the color cuts of $1.30 < \mathrm{F090W} - \mathrm{F150W} < 1.75$ mag, and the horizontal red line and value show the location of the measured TRGB using $s = 0.10$ mag. The blue curve shows the smoothed ($s = 0.10$ mag) luminosity function (LF). The orange and red curves show the response of the Sobel filter applied on luminosity functions binned in 0.01 mag intervals (black) using smoothing values of 0.05 and 0.10 mag, respectively. EDR in the legend refers to the edge detector response using a Sobel filter.

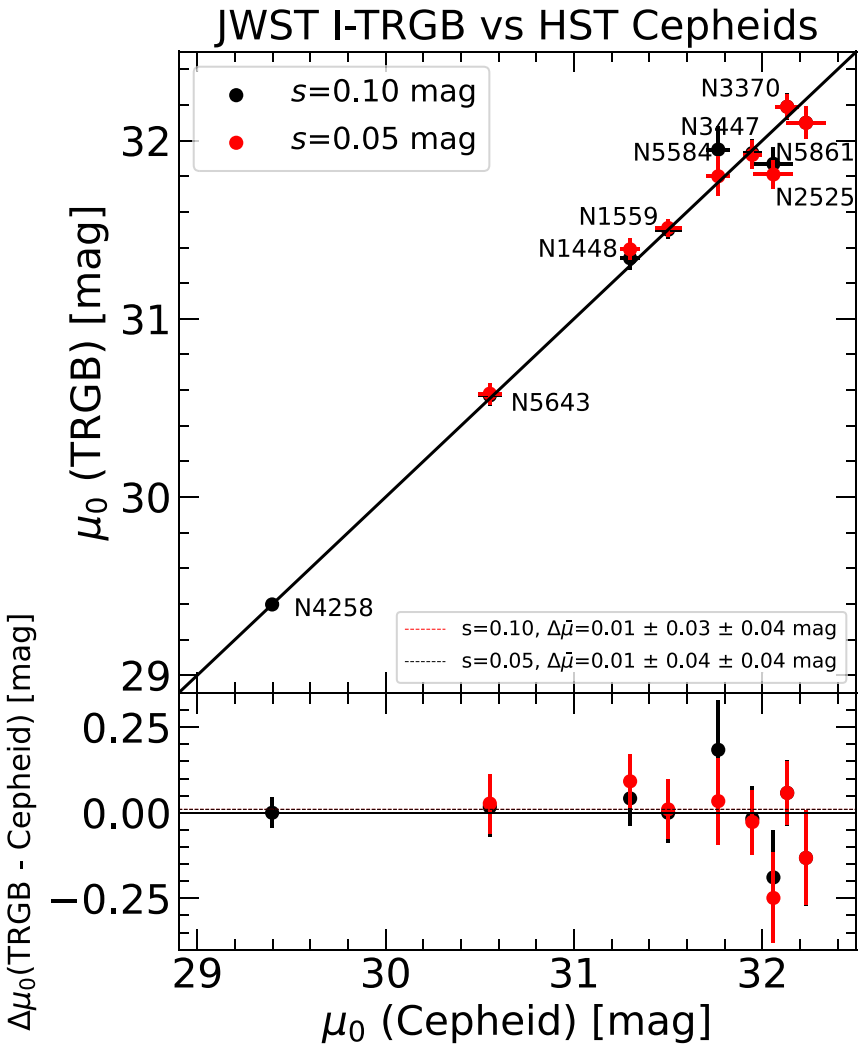

Figure 4. Comparison between the TRGB distances to NGC 1448, NGC 1559, NGC 2525, NGC 3370, NGC 3447, NGC 5584, NGC 5643, and NGC 5861 from this study and the Cepheid-based distances from A. G. Riess et al. (2022; fit variant 10). We compare to fit variant 10 from A. G. Riess et al. (2022) for consistency of using only NGC 4258 as a geometric reference. The top panel plots the TRGB distance moduli as a function of the Cepheid distance moduli. The bottom panel shows the residuals. The red and black points use TRGB measurements with 0.05 and 0.10 mag, respectively. The distance errors do not include a systematic error of 0.032 mag from the common anchor NGC 4258 (M. J. Reid et al. 2019). The weighted means shown include the variants error from Table 2 added in quadrature.

6. Discussion

We measure F090W TRGB-based distances to NGC 1448, NGC 1559, NGC 2525, NGC 3370, NGC 3447, NGC 5584, NGC 5643, and NGC 5861 using JWST NIRCam observations and test their consistency with HST Cepheid-based distances to those same galaxies. We find excellent agreement between the two independent sets of distance measurements, which were measured between the same hosts and anchor but using data taken with different telescopes and distance indicators.

Examining the Hubble Tension necessitates close scrutiny of the consistency and systematics of distance indicators. Based on the measurements made in this study, we find no evidence of a bias or systematic difference between the Cepheid and TRGB methods that would cause a difference translatable to H_0 that can solve the Hubble Tension. This finding is in agreement with W. L. Freedman & B. F. Madore (2023), who find "the excellent agreement between the published Cepheid distances in A. G. Riess et al. (2022) and TRGB distances in W. L. Freedman et al. (2021), which in the mean, agree to 0.007 mag." While the recent analysis in W. L. Freedman et al. (2024) found a 2.5% disagreement between TRGB and Cepheid distances, they do not include systematic measurement errors in NGC 4258 for the two standard candles of 0.04 and 0.09 mag, respectively. Sufficiently accounting for these terms in their comparison decreases the difference to below 1σ and provides no evidence of a significant systematic difference (see Appendix B in A. G. Riess et al. 2024b). In addition, Figure 5 shows a comparison between Cepheid and TRGB distances, both measured with HST, using TRGB and Cepheid distances from W. L. Freedman (2021) and A. G. Riess et al. (2022), respectively. The TRGB and Cepheid distances in Figure 5 yield a mean difference of 0.00 ± 0.02 (stat) ± 0.04 (sys) mag, also consistent with no difference even without additional consideration of populations differences in TRGB measurements (R. I. Anderson et al. 2024; N. W. Koblischke & R. I. Anderson 2024). This comparison will benefit from more JWST TRGB measurements in the future (for instance, from GO-1995; W. L. Freedman et al. 2021). As the Hubble Tension corresponds to $5\log_{10}(73/67.5) \sim 0.17$ mag, the demonstrated

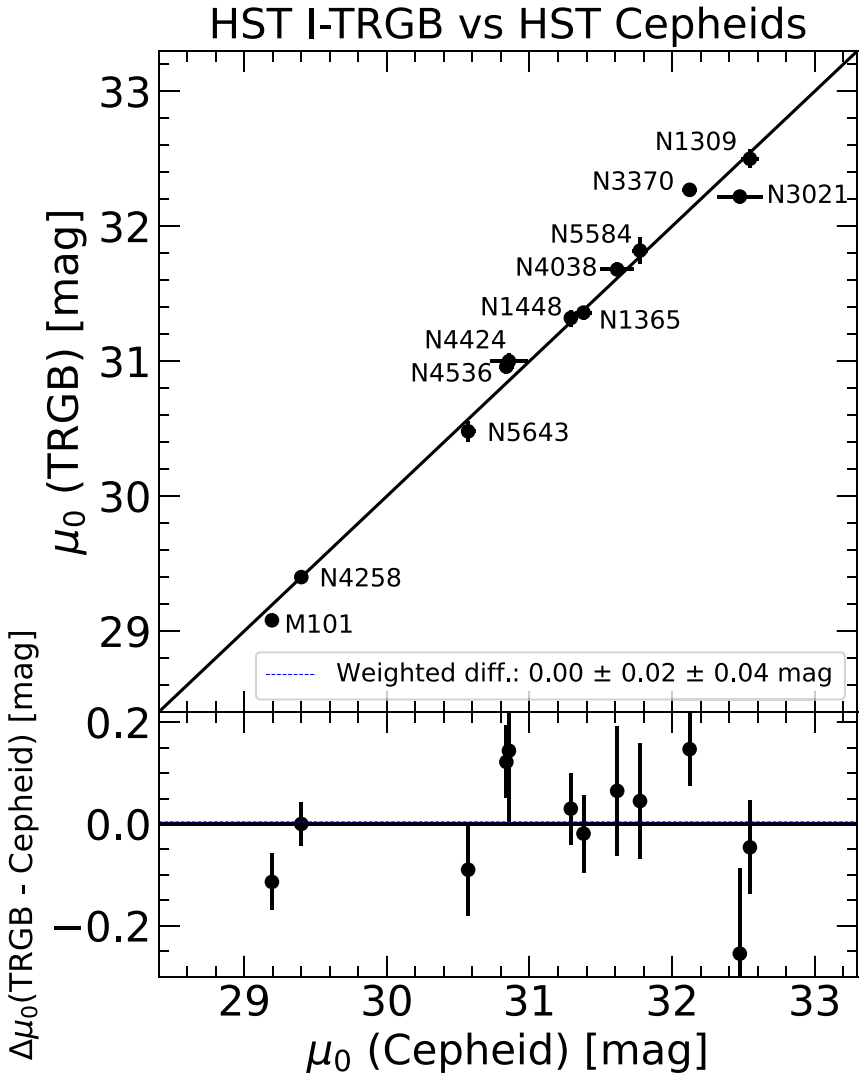

Figure 5. Comparison between the distances to M101, NGC 5643, NGC 4536, NGC 4424, NGC 1448, NGC 1365, NGC 4038, NGC 5584, NGC 3370, NGC 3021, and NGC 1309 based on TRGB (W. L. Freedman 2021) and Cepheids (A. G. Riess et al. 2022). We add the distance to NGC 4258 using the water maser from M. J. Reid et al. (2019) for reference. The distance errors do not include a systematic error of 0.032 mag from the common anchor NGC 4258 (M. J. Reid et al. 2019).

consistency is meaningful and is inconsistent with providing evidence for a solution to the Hubble Tension at 3σ.

We do not yet report a value of H_0 from the JWST-calibrated SN subsamples because they are too small and the anchors too few to be competitive with the HST sample of 42 SNe Ia and 4 anchors. The uncertainty in H_0 would be 2.5 times greater with $\sigma \sim 2$–$2.5\,\mathrm{km\,s^{-1}\,Mpc^{-1}}$ versus $0.9\,\mathrm{km\,s^{-1}\,Mpc^{-1}}$ for HST, which would trivially remove the Hubble Tension simply by inflating the error in H_0. Rather, the greater power of these presently small JWST samples comes from a direct comparison of what they can both measure in common: the distances between the same anchor and SN hosts.

It will be important to also scrutinize the difference in direct H_0 measurements that arise from different treatments of SNe Ia. D. Scolnic et al. (2023) find that the addition of peculiar flow corrections and cross calibration of data sets that are included in the Pantheon and Pantheon+ analyses increase H_0 measurements each by 0.5 and $1.1\,\mathrm{km\,s^{-1}\,Mpc^{-1}}$, respectively, from the W. L. Freedman (2021) analysis, bringing it closer in line with the value obtained from Cepheids. An under-recognized source of variations in determinations of H_0 is also the makeup of the SN Ia calibration sample, which can produce fluctuations of $\sim$1–$2\,\mathrm{km\,s^{-1}\,Mpc^{-1}}$ due to small sample statistics.

Cross-checks between standard candles can be made more comprehensive with additional, independent standard candles such as Miras and carbon stars. The carbon star method, also called the *J*-region Asymptotic Giant Branch (JAGB), originated in the 1980s (H. B. Richer 1981; H. B. Richer et al. 1984, 1985; K. H. Cook et al. 1986; C. J. Pritchet et al. 1987) and has since been revived and further pioneered in the 2000s (P. Battinelli & S. Demers 2005; W. L. Freedman & B. F. Madore 2020; B. F. Madore & W. L. Freedman 2020; P. Ripoche et al. 2020; A. J. Lee et al. 2021a, 2021b, 2022, 2024; J. Parada et al. 2021, 2023; B. Zgirski et al. 2021; B. F. Madore et al. 2022; A. J. Lee 2023; Lee et al. 2024; S. Li et al. 2024). Although the JAGB method still requires further development and standardization (see discussions of asymmetric luminosity functions and metallicity effects in J. Parada et al. 2021, 2023; S. Li et al. 2024), the great luminosities of carbon stars in the NIR allow the JAGB to reach farther than the *I*- and *J*-band TRGB, potentially allowing for a more comprehensive cross-check of Cepheid variables via galaxy distances.

The TRGB measurements made here can benefit from further analysis, such as a future contrast ratio calibration (see CATs; S. Li et al. 2023b; D. Scolnic et al. 2023; J. Wu et al. 2023) or via modeling of the luminosity function (D. Makarov et al. 2006; G. S. Anand et al. 2019b, 2024a) instead of edge-detection algorithms (G. S. Anand et al. 2024, in preparation). However, even without these additions, the consistency of the TRGB-based distance measurements with those of Cepheid-based distances measurement does not show evidence of a bias or systematic offset in Cepheid distances that would resolve the Hubble Tension. Similar analyses in the future will also benefit from further studies investigating the effects of red giant diversity to improve the accuracy of TRGB distances (such as in R. I. Anderson et al. 2024; N. W. Koblischke & R. I. Anderson 2024). Future observations of TRGB fields with HST (for instance, from GO-17520; L. Breuval et al. 2023), JWST, and the Roman Space Telescope will provide more opportunities to scrutinize the second rung of the distance ladder by providing a more extensive set of observations that can be used to compile a more comprehensive comparison between these distance indicators. Specifically, wide-field JWST observations within the anchor galaxy NGC 4258 will help reduce systematic uncertainties with regard to the absolute calibration of the TRGB, and deep JWST observations of galaxies with the highest levels of mismatch between HST Cepheid and HST TRGB distances (e.g., NGC 3021, NGC 4038/9; I. S. Jang & M. G. Lee 2017b) will help elucidate any individual discrepancies between the two techniques. Lastly, a fully independent distance ladder from the traditional Cepheid+SN Ia route is also under construction via the usage of the TRGB combined with surface-brightness fluctuations as the final rung (G. S. Anand et al. 2024b).

Acknowledgments

We are indebted to all of those who spent years and even decades bringing JWST to fruition. We thank Yukei Murakami for the helpful conversations. S.L. is supported by the National Science Foundation Graduate Research Fellowship Program under grant No. DGE2139757. G.S.A. acknowledges financial support from JWST GO-1685 and JWST GO-2875. D.S. is supported by Department of Energy grant DE-SC0010007, the David and Lucile Packard Foundation, and the Templeton Foundation and Sloan Foundation. R.L.B. is supported by the National Science Foundation through grant No. AST-2108616. R.I.A. is funded by the SNSF through an Eccellenza Professorial Fellowship, grant No. PCEFP2_194638.

This research made use of the NASA Astrophysics Data System. This work is based on observations made with the NASA/ESA/CSA JWST. The data were obtained from the Mikulski Archive for Space Telescopes at the Space Telescope Science Institute, which is operated by the Association of Universities for Research in Astronomy, Inc., under NASA contract NAS 5-03127 for JWST. These observations are associated with programs #1685 and #2875. The JWST data presented in this article were obtained from the Mikulski Archive for Space Telescopes (MAST) at the Space Telescope Science Institute. The specific observations analyzed can be accessed via doi:10.17909/556t-7522.

The Digitized Sky Surveys were produced at the Space Telescope Science Institute under U.S. Government grant NAG W-2166. The images of these surveys are based on photographic data obtained using the Oschin Schmidt Telescope on Palomar Mountain and the UK Schmidt Telescope. The plates were processed into the present compressed digital form with the permission of these institutions.

Facility: JWST (NIRCam).

Software: Astropy (Astropy Collaboration et al. 2013, 2018, 2022), SAOImage (W. A. Joye & E. Mandel 2003), DOLPHOT (A. E. Dolphin 2000; A. Dolphin 2016; D. R. Weisz et al. 2024).

ORCID iDs

Siyang Li https://orcid.org/0000-0002-8623-1082
Gagandeep S. Anand https://orcid.org/0000-0002-5259-2314
Adam G. Riess https://orcid.org/0000-0002-6124-1196
Wenlong Yuan https://orcid.org/0000-0001-9420-6525
Louise Breuval https://orcid.org/0000-0003-3889-7709
Lucas M. Macri https://orcid.org/0000-0002-1775-4859
Daniel Scolnic https://orcid.org/0000-0002-4934-5849
Rachael Beaton https://orcid.org/0000-0002-1691-8217
Richard I. Anderson https://orcid.org/0000-0001-8089-4419

References

Anand, G. S., Lee, J. C., Van Dyk, S. D., et al. 2021a, MNRAS, 501, 3621
Anand, G. S., Riess, A. G., Yuan, W., et al. 2024a, ApJ, 966, 89
Anand, G. S., Rizzi, L., Tully, R. B., et al. 2021b, AJ, 162, 80
Anand, G. S., Tully, R. B., Cohen, Y., et al. 2024b, ApJ, 973, 83
Anand, G. S., Tully, R. B., Rizzi, L., & Karachentsev, I. D. 2019a, ApJL, 872, L4
Anand, G. S., Tully, R. B., Rizzi, L., Shaya, E. J., & Karachentsev, I. D. 2019b, ApJ, 880, 52
Anand, G. S., Tully, R. B., Rizzi, L., Riess, A. G., & Yuan, W. 2022, ApJ, 932, 15
Anderson, R. I., Koblischke, N. W., & Eyer, L. 2024, ApJL, 963, L43
Astropy Collaboration, Price-Whelan, A. M., Lim, P. L., et al. 2022, ApJ, 935, 167
Astropy Collaboration, Price-Whelan, A. M., Sipőcz, B. M., et al. 2018, AJ, 156, 123
Astropy Collaboration, Robitaille, T. P., Tollerud, E. J., et al. 2013, A&A, 558, A33
Battinelli, P., & Demers, S. 2005, A&A, 442, 159
Beaton, R. L., Freedman, W. L., Madore, B. F., et al. 2016, ApJ, 832, 210
Beaton, R. L., Seibert, M., Hatt, D., et al. 2019, ApJ, 885, 141
Bellazzini, M., Ferraro, F. R., Sollima, A., Pancino, E., & Origlia, L. 2004, A&A, 424, 199
Blakeslee, J. P., Jensen, J. B., Ma, C.-P., Milne, P. A., & Greene, J. E. 2021, ApJ, 911, 65
Breuval, L., Riess, A., Anand, G. S., et al. 2023, HST Proposal, 31, 17520
Breuval, L., Riess, A. G., Casertano, S., et al. 2024, ApJ, 973, 30
Cook, K. H., Aaronson, M., & Norris, J. 1986, ApJ, 305, 634
Crnojević, D., Sand, D. J., Bennet, P., et al. 2019, ApJ, 872, 80
Dalcanton, J. J., Williams, B. F., Melbourne, J. L., et al. 2012, ApJS, 198, 6
de Vaucouleurs, G., de Vaucouleurs, A., Corwin, H. G., Jr., et al. 1991, Third Reference Catalogue of Bright Galaxies (New York: Springer)
Dhawan, S., Goobar, A., Johansson, J., et al. 2022, ApJ, 934, 185
Dhawan, S., Thorp, S., Mandel, K. S., et al. 2023, MNRAS, 524, 235
Di Valentino, E., Mena, O., Pan, S., et al. 2021, CQGra, 38, 153001
Di Valentino, E., & Brout, D. 2024, The Hubble Constant Tension (Singapore: Springer),
Dolphin, A., 2016 DOLPHOT: Stellar Photometry v2.0, Astrophysics Source Code Library, ascl:1608.013
Dolphin, A. E. 2000, PASP, 112, 1383
Fitzpatrick, E. L. 1999, PASP, 111, 63
Freedman, W. L. 2021, ApJ, 919, 16
Freedman, W. L., & Madore, B. F. 2020, ApJ, 899, 67
Freedman, W. L., & Madore, B. F. 2023, JCAP, 2023, 050
Freedman, W. L., Madore, B. F., Hatt, D., et al. 2019, ApJ, 882, 34
Freedman, W. L., Madore, B. F., Hoyt, T., et al. 2021, JWST Proposal. Cycle, 1, 1995
Freedman, W. L., Madore, B. F., Jang, I. S., et al. 2024, arXiv:2408.06153

Gaia Collaboration, Brown, A. G. A., Vallenari, A., et al. 2021, A&A, 649, A1
Graczyk, D., Pietrzyński, G., Thompson, I. B., et al. 2020, ApJ, 904, 13
Hatt, D., Beaton, R. L., Freedman, W. L., et al. 2017, ApJ, 845, 146
Hoyt, T. J., Beaton, R. L., Freedman, W. L., et al. 2021, ApJ, 915, 34
Hoyt, T. J., Freedman, W. L., Madore, B. F., et al. 2018, ApJ, 858, 12
Hoyt, T. J., Jang, I. S., Freedman, W. L., et al. 2024, ApJ, 975, 111
Huang, C. D., Riess, A. G., Yuan, W., et al. 2020, ApJ, 889, 5
Jang, I. S., & Lee, M. G. 2017a, ApJ, 835, 28
Jang, I. S., & Lee, M. G. 2017b, ApJ, 836, 74
Joye, W. A., & Mandel, E. 2003, in ASP Conf. Ser. 295, Astronomical Data Analysis Software and Systems XII, ed. H. E. Payne, R. I. Jedrzejewski, & R. N Hook (San Francisco, CA: ASP), 489
Kim, Y. J., Kang, J., Lee, M. G., & Jang, I. S. 2020, ApJ, 905, 104
Koblischke, N. W., & Anderson, R. I. 2024, ApJ, 974, 181
Lee, A. J. 2023, ApJ, 956, 15
Lee, A. J., Freedman, W. L., Jang, I. S., Madore, B. F., & Owens, K. A. 2024, ApJ, 961, 132
Lee, A. J., Freedman, W. L., Madore, B. F., Owens, K. A., & Sung Jang, I. 2021a, ApJ, 923, 157
Lee, A. J., Freedman, W. L., Madore, B. F., et al. 2021b, ApJ, 907, 112
Lee, A. J., Rousseau-Nepton, L., Freedman, W. L., et al. 2022, ApJ, 933, 201
Lee, M. G., Freedman, W. L., & Madore, B. F. 1993, ApJ, 417, 553
Li, S., Casertano, S., & Riess, A. G. 2022, ApJ, 939, 96
Li, S., Casertano, S., & Riess, A. G. 2023a, ApJ, 950, 83
Li, S., Riess, A. G., Casertano, S., et al. 2024, ApJ, 966, 20
Li, S., Riess, A. G., Scolnic, D., et al. 2023b, ApJ, 956, 32
Madore, B. F., & Freedman, W. L. 2020, ApJ, 899, 66
Madore, B. F., & Freedman, W. L. 2024, ApJ, 961, 166
Madore, B. F., Freedman, W. L., Hatt, D., et al. 2018, ApJ, 858, 11
Madore, B. F., Freedman, W. L., Lee, A. J., & Owens, K. 2022, ApJ, 938, 125
Makarov, D., Makarova, L., Rizzi, L., et al. 2006, AJ, 132, 2729
Mazzei, P., Marino, A., Rampazzo, R., et al. 2018, A&A, 610, A8
McQuinn, K. B. W., Boyer, M., Skillman, E. D., & Dolphin, A. E. 2019, ApJ, 880, 63
Newman, M. J. B., McQuinn, K. B. W., Skillman, E. D., et al. 2024a, ApJ, 966, 175
Newman, M. J. B., McQuinn, K. B. W., Skillman, E. D., et al. 2024b, ApJ, 966, 175
Oakes, E. K., Hoyt, T. J., Freedman, W. L., et al. 2022, ApJ, 929, 116
Parada, J., Heyl, J., Richer, H., Ripoche, P., & Rousseau-Nepton, L. 2021, MNRAS, 501, 933
Parada, J., Heyl, J., Richer, H., Ripoche, P., & Rousseau-Nepton, L. 2023, MNRAS, 522, 195
Pietrzyński, G., Graczyk, D., Gallenne, A., et al. 2019, Natur, 567, 200
Planck Collaboration, Aghanim, N., Akrami, Y., et al. 2020, A&A, 641, A6
Pritchet, C. J., Richer, H. B., Schade, D., Crabtree, D., & Yee, H. K. C. 1987, ApJ, 323, 79
Reid, M. J., Pesce, D. W., & Riess, A. G. 2019, ApJL, 886, L27
Richer, H. B. 1981, ApJ, 243, 744
Richer, H. B., Crabtree, D. R., & Pritchet, C. J. 1984, ApJ, 287, 138
Richer, H. B., Pritchet, C. J., & Crabtree, D. R. 1985, ApJ, 298, 240
Riess, A., Anderson, R. I., Breuval, L., et al. 2021, JWST Proposal, 1, 1685
Riess, A., Anderson, R. I., Breuval, L., et al. 2023, JWST Proposal, 2, 2875
Riess, A. G., Anand, G. S., Yuan, W., et al. 2024a, ApJL, 962, L17
Riess, A. G., Scolnic, D., Anand, G. S., et al. 2024b, arXiv:2408.11770
Riess, A. G., Yuan, W., Macri, L. M., et al. 2022, ApJL, 934, L7
Ripoche, P., Heyl, J., Parada, J., & Richer, H. 2020, MNRAS, 495, 2858
Rizzi, L., Tully, R. B., Makarov, D., et al. 2007, ApJ, 661, 815
Rizzi, L., Tully, R. B., Shaya, E. J., Kourkchi, E., & Karachentsev, I. D. 2017, ApJ, 835, 78
Schlafly, E. F., & Finkbeiner, D. P. 2011, ApJ, 737, 103
Scolnic, D., Riess, A. G., Wu, J., et al. 2023, ApJL, 954, L31
Tran, Q. H., Hoyt, T. J., Freedman, W. L., et al. 2022, ApJ, 935, 34
Verde, L., Schöneberg, N., & Gil-Marín, H. 2024, ARA&A, 62, 287
Weisz, D. R., Dolphin, A. E., Savino, A., et al. 2024, ApJS, 271, 47
Wu, J., Scolnic, D., Riess, A. G., et al. 2023, ApJ, 954, 87
Wu, P.-F., Tully, R. B., Rizzi, L., et al. 2014, AJ, 148, 7
Zgirski, B., Pietrzyński, G., Gieren, W., et al. 2021, ApJ, 916, 19